Cellular/Molecular

Alterations in Ca^{2+}-Buffering in Prion-Null Mice: Association with Reduced Afterhyperpolarizations in CA1 Hippocampal Neurons

Andrew D. Powell,[1] Emil C. Toescu,[2] John Collinge,[3] and John G. R. Jefferys[1]

Divisions of [1]Neuroscience (Neurophysiology) and [2]Medical Sciences (Physiology), The Medical School, University of Birmingham, Edgbaston, Birmingham B15 2TT, United Kingdom, and [3]Medical Research Center Prion Unit, Department of Neurodegenerative Disease, UCL Institute of Neurology, Queen Square, London WC1N 3BG, United Kingdom

Prion protein (PrP) is a normal component of neurons, which confers susceptibility to prion diseases. Despite its evolutionary conservation, its normal function remains controversial. PrP-deficient (*Prnp*$^{0/0}$) mice have weaker afterhyperpolarizations (AHPs) in cerebellar and hippocampal neurons. Here we show that the AHP impairment in hippocampal CA1 pyramidal cells is selective for the slow AHP, and is not caused by an impairment of either voltage-gated Ca^{2+} channels or Ca^{2+}-activated K^+ channels. Instead, *Prnp*$^{0/0}$ neurons have twofold to threefold stronger Ca^{2+} buffering and double the Ca^{2+} extrusion rate. In *Prnp*$^{0/0}$ neurons thapsigargin abolished the stronger Ca^{2+} buffering and extrusion, and thapsigargin or cyclopiazonic acid abolished the weakening of the slow AHPs. These data implicate sarcoplasmic/endoplasmic reticulum calcium ATPase in the enhanced Ca^{2+} buffering, and extrusion into the endoplasmic reticulum, which contains substantial amounts of PrP in wild-type mice. Altered Ca^{2+} homeostasis can explain several phenotypes identified in *Prnp*$^{0/0}$ mice.

Key words: **calcium signaling; endoplasmic reticulum; AHP; hippocampus; prion; transgenic**

Introduction

Prion protein (PrP) is a widely expressed plasma membrane-associated glycoprotein with highest levels of expression on neurons and glia. It is widely accepted that an abnormal isoform of this protein underlies transmissible spongiform encephalopathies such as bovine spongiform encephalopathy, scrapie, and Creutzfeldt-Jakob disease (Prusiner, 1998; Collinge, 2001). Despite the central role of PrP in these diseases, and its evolutionary conservation, its normal function remains unclear. A proposed role for PrP is metal ion homeostasis (Brown, 2002; Watt and Hooper, 2003) because it binds copper avidly although its functional consequences, if any, are unclear (Davies and Brown, 2008). Other proposed roles for PrP include protection from oxidative stress (Brown, 2002; Krebs et al., 2007), although this is contentious (Hutter et al., 2003; Jones et al., 2005), and signal transduction (Rieger et al., 1997; Chiarini et al., 2002). In the brain, PrP particularly localizes to synaptic membranes (Herms et al., 1999; Fournier et al., 2000), suggesting a role in neurotransmission. This hypothesis supported by several reports of subtle alterations in neuronal function in PrP-deficient (*Prnp*$^{0/0}$) mice. These alterations include mossy fiber reorganization (Colling et al., 1997), reduced long-term potentiation (LTP) (Collinge et al., 1994; Manson et al., 1995), decreased EPSPs (Carleton et al., 2001), and reduced synaptic inhibition (Collinge et al., 1994). A reproducible electrophysiological phenotype is a reduction in the slow afterhyperpolarization (AHP) (Colling et al., 1996; Herms et al., 2001; Mallucci et al., 2002; Fuhrmann et al., 2006). The slow AHP is a property found in many neurons, which is evoked by repetitive action potentials, can last for several seconds and reduces the likelihood of subsequent action potential firing (Lancaster and Adams, 1986). The slow AHP is mediated by a Ca^{2+}-dependent K^+ channel, the exact molecular identity of which remains elusive (Sah and Clements, 1999; Bond et al., 2004; Pedarzani et al., 2005). The observed weaker slow AHP in PrP-deficient mice has several potential mechanisms, including impaired function of either Ca^{2+} or K^+ channels, disruption of their interaction, or altered Ca^{2+} homeostasis.

Herms et al. (Fuhrmann et al., 2006) suggested that the reduction in slow AHP is caused by an alteration in L-type voltage-gated Ca^{2+} channels (VGCCs) in CA1 hippocampal neurons. Whether this mechanism is sufficient to explain the observed alterations in Ca^{2+} signaling in diverse cell types remains unclear. In cerebellar granule neurons, basal levels and depolarization-induced Ca^{2+} signals are reduced without observed alterations in VGCC function (Herms et al., 2000). Prion protein expression has also been shown to have profound effects on Ca^{2+} signaling in Chinese hamster ovary cells (Brini et al., 2005).

Received May 11, 2007; accepted Feb. 24, 2008.

This work was supported by Biotechnology and Biological Sciences Research Council Project Grant 6/BS5 16776 to J.G.R.J. and J.C. We thank the members of the Department of Neurophysiology and Drs. Frank Michelangeli and Graham Jackson for invaluable discussions. The assistance of Karin Swerdya and Gail O'Brian in the maintenance of the mice colonies is gratefully acknowledged.

Correspondence should be addressed to John G. R. Jefferys at the above address. E-mail: J.G.R.Jefferys@bham.ac.uk.

DOI:10.1523/JNEUROSCI.0675-08.2008

 0270-6474/08/283877-10$15.00/0

In the present study, we examined the effect of PrP expression on the Ca^{2+} homeostasis of CA1 pyramidal neurons to find a mechanism that can explain the reduction in both Ca^{2+} signaling and the slow AHP. By use of patch-clamp recordings of individual hippocampal CA1 pyramidal neurons, we examined the mechanism of the reduction in slow AHP and correlated this with changes in Ca^{2+} signaling.

Materials and Methods

Origin and use of $Prnp^{0/0}$ *mice.* Mice were bred at the University of Birmingham from progenitor mice supplied by the Medical Research Council Prion Unit (London, UK). Two groups of mice were used: homozygous PrP-null (*Prnp*$^{0/0}$) and wild-type controls (*Prnp*$^{+/+}$). The PrP-null mice were generated from "Zurich 1" mice (Bueler et al., 1992), fully backcrossed onto an FVB/N background; control mice were inbred FVB/N mice bred in the same unit. All experiments and analysis were performed blind to the genotype of the mice.

Preparation and maintenance of acute hippocampal slices. A total of 47 *Prnp*$^{+/+}$ and 49 *Prnp*$^{0/0}$ age-matched male mice (3–9 weeks old) were anesthetized by intraperitoneal injection of a mixture of medetomidine (1 mg/kg) and ketamine (76 mg/kg), before being killed by cervical dislocation. The brains were rapidly removed and chilled (<3°C), in oxygenated, ice-cold sucrose-based cutting solution composed of (in mM) 189 sucrose, 26 $NaHCO_3$, 1.2 NaH_2PO_4, 2.5 KCl, 0.1 $CaCl_2$, 5 $MgCl_2$, and 10 glucose. The brains were cut along the midline, and 300 μm horizontal hippocampal slices were cut using an Integraslice (Campden Instruments, Loughborough, UK). Hippocampal slices were maintained at room temperature in an interface storage chamber containing 95%O_2–5%CO_2 oxygenated aCSF. The composition of the artificial CSF (aCSF) was (in mM) 135 NaCl, 16 $NaHCO_3$, 1.25 NaH_2PO_4, 3 KCl, 2 $CaCl_2$, 1 $MgCl_2$ and 10 glucose, pH 7.4.

Slices were transferred to a recording chamber, where they were submerged and continually perfused (4–5 ml/min) with warm (29–31°C) aCSF, bubbled with 95%O_2–5%CO_2. Slices were allowed to equilibrate in the aCSF solution for >10 min before recording. Slices were changed after ~1 h.

Whole-cell recordings. Whole-cell patch-clamp recordings were made from the somata of CA1 pyramidal neurons using infrared differential interference contrast on an Olympus (Tokyo, Japan) BX-51 upright microscope, fitted with a fluorplan 40×, 0.8 numerical aperture water-immersion lens (Micro Instruments, Long Hanborough, UK). CA1 neurons were visually selected based on appearance and the integrity of the apical dendrites (visible for ~100 μm from the soma). Patch electrodes were pulled from borosilicate glass capillaries (outer diameter, 1.2 mm; inner diameter, 0.69 mm; Harvard Apparatus, Edenbridge, UK) using a P-97 horizontal puller (Sutter Instruments, Novato, CA) and filled with intracellular solution comprising (in mM) 135 KCH_3SO_4, 8 NaCl, 10 HEPES, 2 Mg-ATP and 0.3 Na-GTP; adjusted to pH 7.3 with KOH (~285 mOsm), unless stated otherwise. For the VGCC studies, equimolar $CsCH_3SO_4$ replaced KCH_3SO_4 and 1 μM tetrodotoxin was added to the extracellular solution to reduce Na^+ channel activation. For some VGCC studies, the standard aCSF was replaced by a tetraethylammonium chloride (TEA)-based extracellular solution containing (in mM) 148 TEA-Cl, 4 KCl, 2 $CaCl_2$, 1 $MgCl_2$, 10 HEPES, and 0.001 TTX, pH 7.3 with TEA-OH (298 mOsm). Patch electrodes filled with the intracellular solutions typically had resistances of 4–7 MΩ. Membrane potentials and currents were recorded using an NPI SEC-10L amplifier (Scientifica, Harpenden, UK), acquired and digitized at 10 kHz using a Power 1401 A–D converter (Cambridge Electronic Design, Cambridge, UK). Data were low-pass Bessel filtered at 1 kHz by either a Neurolog NL-125 or NL-135 filter unit (Digitimer, Welwyn Garden City, UK) before storage on a computer. Data acquisition and stimulus parameters were controlled using Signal software (version 2.16; Cambridge Electronic Design).

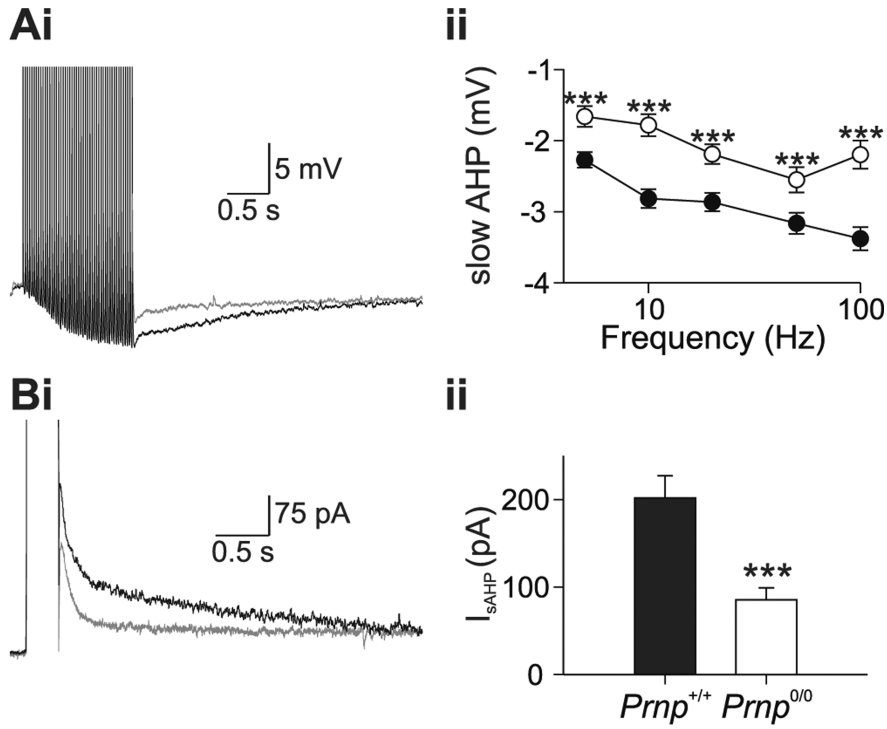

Figure 1. ***A***, $Prnp^{0/0}$ neurons possess a reduced slow afterhyperpolarization. ***Ai***, A train of 50 action potentials at 20 Hz, evoked both a medium and slow AHP in *Prnp*$^{+/+}$ (black traces) and *Prnp*$^{0/0}$ (gray traces) neurons. The medium AHP was defined by its rapid kinetics and was observed immediately after cessation of action potential firing. The slow AHP was defined by its slower kinetics and was smaller in *Prnp*$^{0/0}$ neurons at all frequencies tested (***Aii***). ***B***, A 300 ms depolarization from −65 to +5 mV activated both a medium AHP current (I_{mAHP}), which displayed faster kinetics and was observed immediately after cessation of the depolarization and slow AHP current (I_{sAHP}) which displayed slower kinetics. Similar to the slow afterhyperpolarization, the I_{sAHP} was smaller in *Prnp*$^{0/0}$ neurons. ***$p < 0.001$.

Epifluorescent Ca^{2+} *measurements.* Hippocampal CA1 neurons were loaded, via the patch pipette, with the Ca^{2+} indicator dyes, Fura-2 or Fluo-3 as indicated in the text (Invitrogen, Eugene, OR). Epifluorescence measurements were performed using a dual photomultiplier tube (PMT) system (Cairn Research, Faversham, Kent, UK) mounted onto the microscope. The fluorophore was excited with light of an appropriate wavelength (Fura-2, 340 and 380 nm; Fluo-3, 488 nm), using a computer controlled Optoscan monochromator (Cairn Research). Emitted light was selected using either a 510 ± 20 nm filter for Fura-2 or a 535 ± 20 nm filter for Fluo-3 (Chroma Technologies, Rockingham, VT). The outputs of the PMTs were sampled at 200 Hz using Signal (Cambridge Electronic Design) and stored on the computer. Regions of interest (ROIs) were selected by use of adjustable rectangular field stops; one ROI was placed over the somatic region, and a second over the initial 25–75 μm segment of the apical dendrite. Changes in fluorescence were background subtracted using a ROI located close to the cell under investigation. Changes in intracellular Ca^{2+} concentration ($[Ca^{2+}]_i$) were calculated from the Ca^{2+}-dependent F_{340}/F_{380} fluorescence ratio (R), according to Grynkiewicz et al. (1985) (Eq. 1). Calibration constants for Fura-2 were determined by patch clamping CA1 pyramidal neurons (seven neurons per intracellular solution per genotype) with the following intracellular solutions: R_{min} (Ca^{2+}-free), 135 KCH_3SO_4, 8 NaCl, 10 HEPES, 2 Mg-ATP, 0.3 Na-GTP, and 10 BAPTA; R_{400} (400 nM free Ca^{2+}), 135 KCH_3SO_4, 8 NaCl, 10 HEPES, 2 Mg-ATP, 0.3 Na-GTP, 9.9 BAPTA, and 6.6 $CaCl_2$, yielding a final intracellular Ca^{2+} concentration of 400 nM (calculated

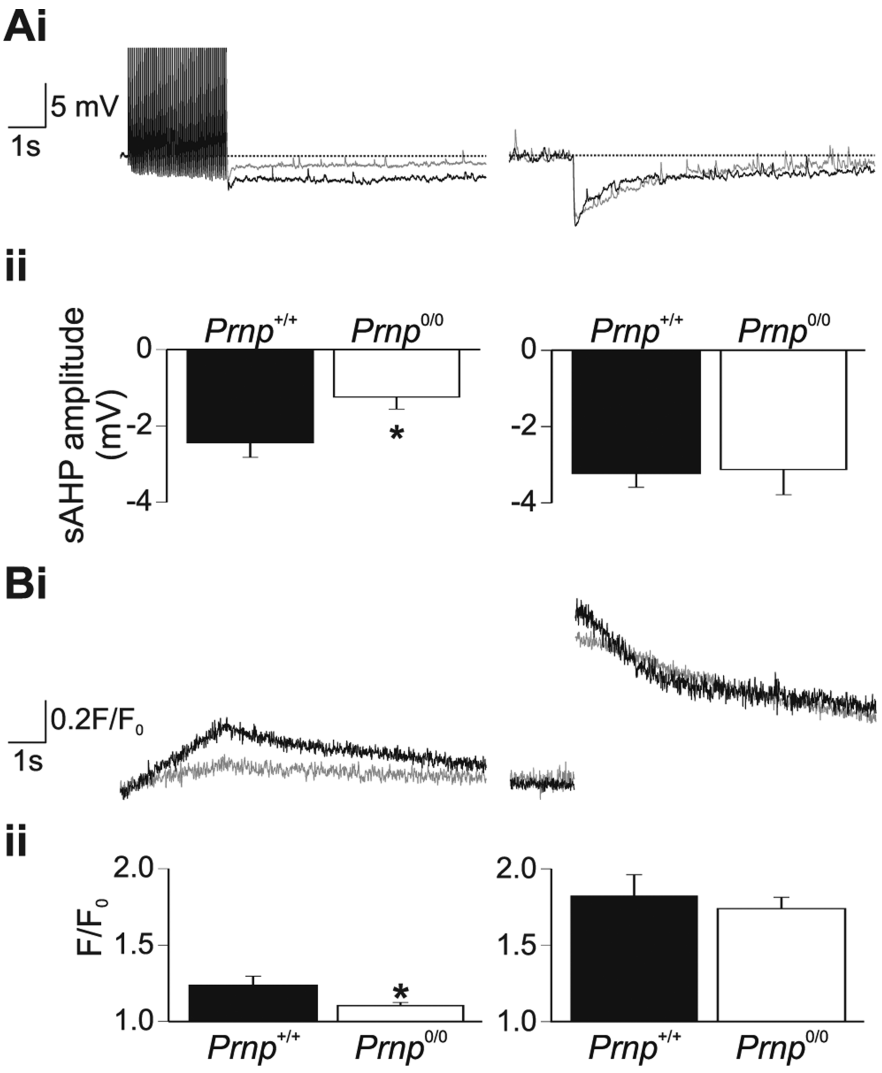

Figure 2. The reduced slow AHP is not caused by alterations in the underlying K^+ channels. Whole-cell recordings were obtained using electrodes filled with internal solution including 100 μM Fluo-3 and 10 mM DM-nitrophen (Ca^{2+} cage). ***A***, ***B***, *Prnp*$^{0/0}$ neurons filled with this solution displayed a significantly reduced action potential evoked slow AHP (***A***, left, gray traces), associated with a significant attenuation of Ca^{2+} increases (***B***, left, gray traces). In contrast, flash photolysis evoked a robust and similar AHP in both *Prnp* $^{+/+}$ and *Prnp*$^{0/0}$ neurons (***A***, right), associated with similar Ca^{2+} transients in the two genotypes (***B***, right). *$p < 0.05$.

using the MaxChelator program, http://www.stanford.edu/~cpatton/maxc.html); R_{max} (10 mM free Ca^{2+}), 135 KCH_3SO_4, 8 NaCl, 10 HEPES, 2 Mg-ATP, 0.3 Na-GTP, and 10 $CaCl_2$. The R_{400} intracellular solution was used to confirm the value of the calibration constant. All intracellular solutions were adjusted to pH 7.3 with KOH. The Ca^{2+} dissociation constant for Fura-2 (K_d) was determined to be 247 nM by using the following equation (Grynkiewicz et al. (1985):

$$[Ca^{2+}]_i = K_d(R_{max}/R_{min})(R - R_{min})(R_{min} - R). \quad (1)$$

To minimize complications associated with diffraction of fluorescent light associated with alterations in cell depth, care was taken to ensure that the same criteria (cell soma; 15–25 μm, < 50 μm depth from slice surface) for cell selection were used to identify CA1 pyramidal neurons used for the Fura-2 calibration experiments. No systematic differences in the K_d were found between *Prnp* $^{+/+}$ and *Prnp*$^{0/0}$ neurons (data not shown).

Analysis of endogenous Ca^{2+} buffering. Calcium homeostasis was quantified by using the "added buffer method," which relies on the ability of Ca^{2+}-sensitive dyes, such as Fura-2, to compete with endogenous buffers and alter the Ca^{2+} dynamics (Neher, 1995; Helmchen et al., 1996; Palecek et al., 1999). Before patch breakthrough the buffering is mediated solely by the neuron's endogenous buffers; after breakthrough, the concentration of exogenous buffer increases until it reaches a point where virtually all Ca^{2+} that enters the cell is sequestered by the exogenous buffer. Ca^{2+} transients were evoked by a 50 ms depolarization (−65 to −5 mV) every 30 s after patch breakthrough. After establishment of the whole-cell recording configuration, the concentration of Fura-2 within the cell increased with time until $[Fura2]_i$ equilibrated with $[Fura2]_{pipette}$ (see Fig. 5*Ai*,*Aii*). The buffering capacity of Fura-2 (κ_B) was calculated using the following equation:

$$\kappa_B = [B]K_d/(([Ca^{2+}]_{basal} + K_d)([Ca^{2+}]_{peak} + K_d)), \quad (2)$$

where [B] and K_d are the concentration and dissociation constant of Fura-2, respectively (Helmchen et al., 1996).

The amplitude (A) and decay rate (τ) of the Ca^{2+} signal are related to the buffering capacity of the endogenous buffer (κ_S) according to Equations 3 and 4 (Helmchen et al., 1996):

$$A = \Delta[Ca^{2+}]_T/(1 + \kappa_S + \kappa_B) \quad (3)$$

$$\tau = (1 + \kappa_S + \kappa_B)/\gamma, \quad (4)$$

where $\Delta[Ca^{2+}]_T$ is the increase in total Ca^{2+} (free and bound) and γ is the Ca^{2+} extrusion rate.

Equations 3 and 4 predict that increases in κ_B will reduce the amplitude and slow the decay kinetics of the Ca^{2+} transient. Both the inverse of the amplitude (A^{-1}) and τ depend linearly on κ_B. The relationship between A^{-1} and κ_B allows estimation of the endogenous Ca^{2+} binding ratio (κ_S), as the negative abscissa intercept. κ_S then allows estimation of γ from Equation 4.

Added buffer measurements were performed on slices from mice over a narrow age range (postnatal days 42–55) to avoid any impact of age (Maravall et al., 2000).

Flash photolysis. DM-nitrophen (Calbiochem, La Jolla, CA) was used as the caged compound for photorelease of Ca^{2+} and was dissolved directly in internal solution in which Mg-ATP was replaced with Na-ATP to avoid Mg^{2+} loading (Faas et al., 2005). DM-nitrophen (10 mM) was 60–70% loaded with Ca^{2+}. The resulting free $[Ca^{2+}]$ was calculated to be ~80 nM using the MaxChelator program. The lamp used for photolysis was a pulsed xenon arc lamp (Cairn Research); flash intensity was controlled by use of a variable capacitance system (20–4070 μF; 400V). The flash illuminated the entire field of view and discharged in <2 ms. For the flash photolysis experiments, it was necessary to use the longer wavelength indicator Fluo-3 (100 μM) to monitor $[Ca^{2+}]_i$ because the UV illumination required to excite Fura-2 fluorescence would also photolyse the DM-nitrophen. For the flash photolysis experiments, because Fluo-3 is not a ratiometric dye, changes in intracellular Ca^{2+} were not calibrated and are expressed as $\Delta F/F_0$.

Data analysis. All values are expressed as mean ± SEM. Curve fitting was performed in Origin 8 (Silverdale Scientific, Stoke Mandeville, UK); statistical analysis was performed in SPSS 13 (SPSS, Woking, UK). Student's *t* tests and ANOVA were used as appropriate and the significant criterion was $p < 0.05$, unless otherwise stated.

Results

To understand the role of prion protein in Ca^{2+} signaling, we examined the relationship between the AHP and Ca^{2+} signaling using a combined electrophysiological and microfluorimetric approach. Previous studies have shown that *Prnp*$^{0/0}$ neurons have a reduced AHP (Colling et al., 1996; Herms et al., 2001; Mallucci et al., 2002; Fuhrmann et al., 2006). Whole-cell patch clamp recordings were made from the somata of CA1 pyramidal neurons and AHPs were evoked either by repetitive action potential firing or by direct activation of voltage-gated Ca^{2+} channels. Figure 1*A* illustrates typical AHPs recorded from *Prnp*$^{+/+}$ and *Prnp*$^{0/0}$ neurons in response to 50 action potentials (delivered at 20Hz). The slow AHP was significantly smaller in *Prnp*$^{0/0}$ neurons than in *Prnp*$^{+/+}$ neurons (2.19 ± 0.13 mV, $n = 17$; 3.05 ± 0.18 mV, $n = 19$, respectively) (Fig. 1*A*). When the slow AHP current (I_{sAHP}) was evoked by activation of voltage-gated Ca^{2+} channels by a depolarizing pulse in voltage-clamp mode, the I_{sAHP} was significantly smaller in *Prnp*$^{0/0}$ neurons than in *Prnp*$^{+/+}$ neurons (85.5 ± 13.5 pA and 201.8 ± 25.3 pA, respectively) (Fig. 1*B*). The apparent reduction in the medium AHP was attributable to the reduction in the underlying slow AHP (supplemental data part 2, available at www.jneurosci.org as supplemental material).

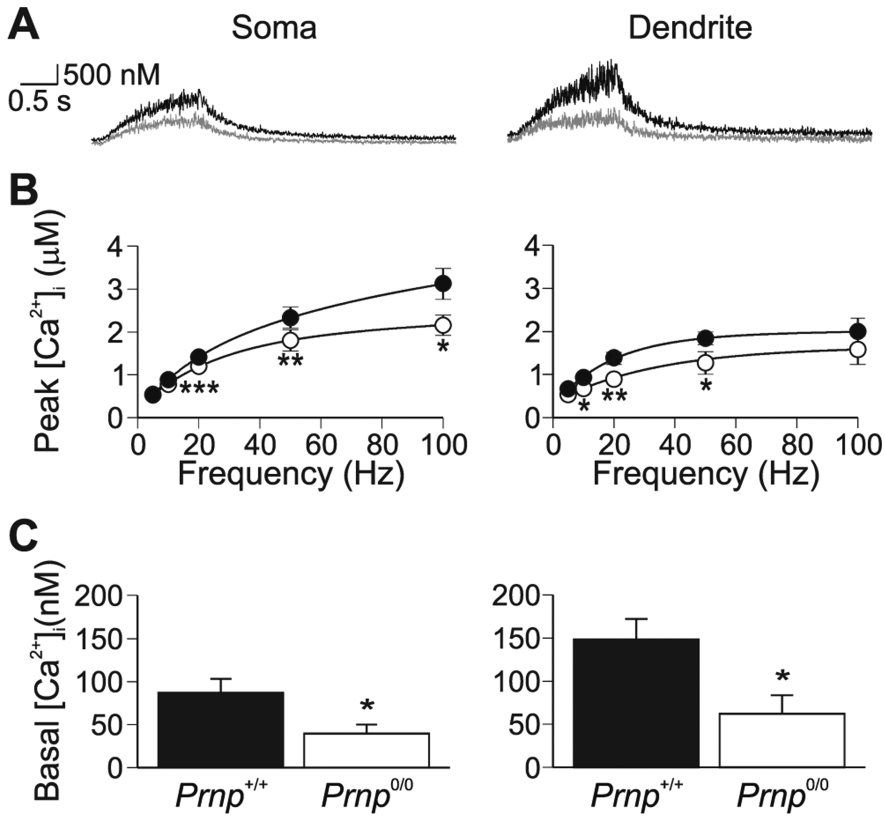

Figure 3. Ca^{2+} signaling is perturbed in *Prnp*$^{0/0}$ neurons. ***A***, *Prnp*$^{0/0}$ neurons (gray traces) produce weaker Ca^{2+} transients, in both somatic (left) and dendritic regions (right), in response to 50 action potentials evoked at 20 Hz. ***B***, Peak Ca^{2+} changes were significantly reduced across the frequency range ($p < 0.001$, ANOVA; ●, *Prnp* $^{+/+}$; ○, *Prnp*$^{0/0}$) for both somatic (left) and dendritic (right) regions. ***C***, The resting Ca^{2+} level was significantly reduced in *Prnp*$^{0/0}$ neurons in both the somatic (left) and proximal dendritic (right) regions. Somatic and dendritic regions were not significantly different. *$p < 0.05$; **$p < 0.01$; ***$p < 0.005$.

We have confirmed that *Prnp*$^{0/0}$ neurons display a selective reduction in the slow AHP in CA1 pyramidal neurons. The slow AHP is mediated by Ca^{2+}-dependent K^+ channels that are activated by Ca^{2+} entry through VGCCs (Sah and Faber, 2002), suggesting several mechanisms for the reduction in the slow AHP amplitude. These include altered Ca^{2+} channel function (Fuhrmann et al., 2006), altered Ca^{2+} signaling (Herms et al., 2000) and altered K^+ channel function.

Flash photolysis

To test the hypothesis that functioning of the K^+ channel that is responsible for the slow AHP is altered in *Prnp*$^{0/0}$ mice, we used photorelease of calcium from DM-nitrophen to elevate intracellular [Ca^{2+}] independently of Ca^{2+} channel activation. This method is well established in the investigation of the molecular basis of the slow AHP (Lancaster and Zucker, 1994; Sah and Clements, 1999).

Action potential firing (50 action potentials at 20 Hz), evoked slow AHPs in both *Prnp*$^{+/+}$ and *Prnp*$^{0/0}$ neurons. *Prnp*$^{+/+}$ neurons had a slow AHP of 2.44 ± 0.38 mV ($n = 5$) (Fig. 2*A*, left). Ca^{2+} concentration, as reported by changes in Fluo-3 fluorescence, increased throughout the period of action potential firing reaching a peak fluorescence value of 1.24 ± 0.06 (Fig. 2*B*, left). *Prnp*$^{0/0}$ neurons generated a significantly smaller slow AHP (1.24 ± 0.31 mV; $n = 6$; $p < 0.05$) (Fig. 2*A*, left). Furthermore, *Prnp*$^{0/0}$ mice produced significantly smaller Ca^{2+} increases in response to action potential firing (peak fluorescence value, 1.10 ± 0.02, $p < 0.05$) (Fig. 2*B*, left). Therefore, under the recording conditions necessary for flash photolysis studies, it is possible to replicate the reduced slow AHP amplitude in *Prnp*$^{0/0}$ neurons. In *Prnp*$^{+/+}$ neurons, flash photolysis of DM-nitrophen evoked a rapid increase in Ca^{2+} concentration (peak value, 1.82 ± 0.14) (Fig. 2*B*, right) and a concomitant membrane hyperpolarization of 3.23 ± 0.36 mV (Fig. 2*A*, right). In *Prnp*$^{0/0}$ neurons, flash photolysis released similar amounts of Ca^{2+} as in wild-type neurons (peak value, 1.74 ± 0.07; $p = 0.58$); the decay rate of the Ca^{2+} signal did not significantly differ between *Prnp*$^{+/+}$ and *Prnp*$^{0/0}$ neurons (τ_{decay} 2.73 ± 1.06 s, $n = 5$ and 2.55 ± 0.96 s, $n = 6$, respectively; $p = 0.76$). The hyperpolarization observed in response photorelease of Ca^{2+} was not significantly different in *Prnp*$^{0/0}$ mice (3.12 ± 0.66 mV; $p = 0.89$). The hyperpolarization activated by flash photolysis of caged Ca^{2+} was confirmed as a slow AHP, because it was inhibited by 5-hydroxytryptamine (10 μM). Moreover, the flash evoked hyperpolarization displayed similar kinetics to the action potential evoked AHPs (supplemental data, part 2, available at www.jneurosci.org as supplemental material).

The AHP in *Prnp*$^{0/0}$ neurons was smaller only when activated by Ca^{2+} entry through Ca^{2+} channels, but not by homogeneous Ca^{2+} elevation resulting from photolysis of intracellular DM-nitrophen. The direct activation of the K^+ channels underlying the slow AHP reveals, for the first time, that they are both present and functioning correctly in *Prnp*$^{0/0}$ neurons. Therefore, alterations in K^+ channel function cannot explain the observed reduction of slow AHP amplitude.

Ca^{2+} signaling

Several studies have implicated changes in Ca^{2+} homeostasis in the absence of PrP (Herms et al., 2000, 2001; Brini et al., 2005; Fuhrmann et al., 2006). The flash photolysis study (Fig. 2*B*, left), suggested that Ca^{2+} homeostasis was altered in the present study. Here we have used single cell fluorimetry with Fura-2 specifically to examine the role of prion protein in Ca^{2+} signaling and buffering.

Resting Ca^{2+} levels in $Prnp^{0/0}$ neurons were lower in both dendritic ($Prnp^{+/+}$, 148.2 ± 23.8 nM; $Prnp^{0/0}$, 62.2 ± 21.4 nM; $p = 0.01$) and somatic regions (86.9 ± 16.1 nM; $Prnp^{0/0}$, 39.5 ± 10.7 nM; $p = 0.03$) (Fig. 3*C*).

Stimulating cells with 50 action potentials at 20 Hz evoked increases in intracellular Ca^{2+} in both the somatic (Fig. 3*A*; left panel) and the proximal dendrite regions (Fig. 3*A*, right panel), with the peak Ca^{2+} concentration occurring at the end of the spike train. The evoked peak [Ca^{2+}] significantly increased with action potential frequency in both somatic and dendritic regions (Fig. 3) (ANOVA $p = 0.01$ and 0.03, respectively). ANOVA revealed that the peak Ca^{2+} increases in $Prnp^{0/0}$ neurons were smaller across a range of frequencies in both the soma and dendrites ($p < 0.001$). We chose to use 50 action potentials at 20 Hz as the standard stimulation protocol because the effective Ca^{2+} range for Fura-2 is ~20 nM–2 μM and both 50 and 100 Hz resulted in Ca^{2+} increases in excess of 2 μM (Fig. 3*B*). Ca^{2+} increases evoked by 50 action potentials at 20 Hz in the dendrites were smaller in $Prnp^{0/0}$ cells than in wild type (0.88 ± 0.11 μM, $n = 10$ and 1.37 ± 0.14 μM, $n = 12$, respectively; $p < 0.01$) (Fig. 3*A*). The peak Ca^{2+} response was similarly smaller in the soma: 1.19 ± 0.10 μM, $n = 16$ in $Prnp^{0/0}$ and 1.41 ± 0.06, $n = 21$ in wild type ($p < 0.005$).

The observed alterations in Ca^{2+} signaling could be explained by changes in VGCC function, as has been reported previously for CA1 pyramidal neurons (Fuhrmann et al., 2006). We investigated this possibility by comparing the voltage dependence of VGCC currents and simultaneously measured Ca^{2+} transients from both $Prnp^{+/+}$ and $Prnp^{0/0}$ neurons. Neurons were voltage clamped at −70 mV and 200 ms step depolarizations (−60 mV to + 30 mV; 10 mV increments) were applied every 30 s. No differences in the *I–V* relationships were observed between $Prnp^{+/+}$ and $Prnp^{0/0}$ neurons whether in bicarbonate-buffered aCSF ($p = 0.89$) (Fig. 4*A*,*B*) or HEPES-buffered aCSF ($p = 0.69$) (supplemental data part 4, available at www.jneurosci.org as supplemental material). Ca^{2+} changes evoked by step depolarizations, however, were significantly smaller in $Prnp^{0/0}$ than in $Prnp^{+/+}$ neurons (1.37 ± 0.18 μM and 2.36 ± 0.32 μM, respectively; $p = 0.03$) (Fig. 4*A*). We have therefore excluded the possibility that the alteration in slow AHP is caused by alterations in either K^+-channel or Ca^{2+}-channel function.

Endogenous Ca^{2+} buffering capacity

We used the "added buffer" technique (Neher, 1995) to investigate whether the PrP-dependent differences in Ca^{2+} signaling, found in this and other studies (Herms et al., 2000; Brini et al., 2005; Fuhrmann et al., 2006), could be explained by changes in endogenous Ca^{2+} binding capacity. Diffusion of Fura-2 from the patch pipette provided controlled loading of Ca^{2+} buffer into the neurons, with simultaneous recording of calcium responses triggered by somatic depolarization (50 ms duration −65 to +5 mV, every 30 s). During Fura-2 loading, the concentration of exogenous Ca^{2+} buffer progressively increases and eventually dominates; the relationship of the Ca^{2+} response with the concentration of Fura-2 allows estimation of Ca^{2+} buffering extrusion (Eqs. 3, 4) (Neher, 1995; Helmchen et al., 1996; Palecek et al., 1999).

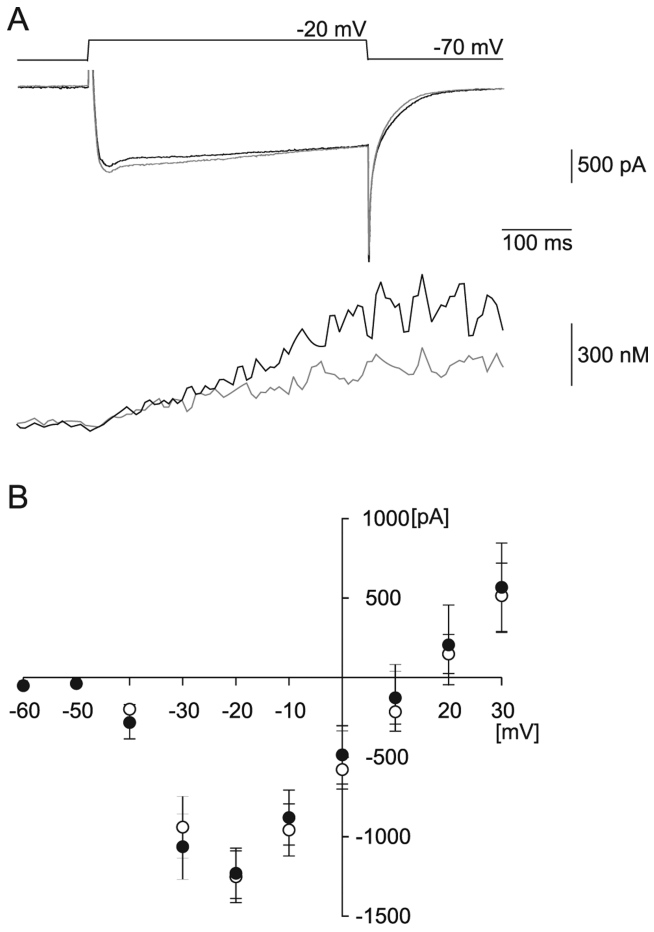

Figure 4. Voltage-gated Ca^{2+} channels are unaffected in $Prnp^{0/0}$ neurons. ***A***, Ca^{2+} current amplitude and kinetics were unaffected in $Prnp^{0/0}$ neurons in response to a 200 ms step depolarization. The Ca^{2+} changes, as monitored by 100 μM Fura-2, were significantly smaller in $Prnp^{0/0}$ neurons (bottom, gray trace) than in $Prnp^{+/+}$ neurons (for statistics, see Results). ***B***, Ca^{2+} current-voltage relationship is not altered in $Prnp^{0/0}$ neurons (●, $Prnp^{+/+}$; ○, $Prnp^{0/0}$).

Fura-2 concentration was estimated from changes in the fluorescence intensity recorded at the isobestic wavelength (358 ± 3 nm in our system), measured every 30 s after establishment of a gigaohm seal (Fig. 5*Ai*,*Aii*). The time course of Fura-2 loading was best fit by a single exponential, and did not differ between wild-type (time constant, 2.8 ± 0.4 min, $n = 8$) and $Prnp^{0/0}$ neurons (time constant, 2.6 ± 0.2 min, $n = 8$) (Fig. 5*Ai*,*Aii*, supplemental Fig. 1*B*, available at www.jneurosci.org as supplemental material). The concentration of Fura-2 was converted to Fura-2 binding ratio (κ'_B) according to the method of Helmchen et al. (1996). Initial series resistance varied between 8 and 12 MΩ; cells were excluded from buffering analysis if the resistance changed by >20% during the recording period. Somatic Ca^{2+} transients were evoked by a 50 ms depolarization every 30 s. Ca^{2+} increases evoked by this stimulation protocol were stable throughout the duration of the Ca^{2+} buffering experiments (supplemental Fig. 1*C*, available at www.jneurosci.org as supplemental material).

Analysis of the amplitude and the decay of the Ca^{2+} transients from eight wild-type and eight $Prnp^{0/0}$ neurons during loading with 100 μM Fura-2 showed that both inverse amplitude and decay rate depended on κ'_B and were best fit by a linear regression (Fig. 5*B*, supplemental Fig. 1*D*, available at www.jneurosci.org as

supplemental material). The integral of the Ca^{2+} change was independent of κ'_B (similar to Helmchen et al., 1996) (supplemental Fig. 1*Diii*, available at www.jneurosci.org as supplemental material). The intercept of the regression line with the ordinate ($\kappa'_B = 0$) provides an estimate of both the Ca^{2+} change and kinetics in the absence of exogenous buffer. The negative abscissa intercept provides an estimate of the endogenous binding capacity (κ_S) (Helmchen et al., 1996). κ_S estimated from the inverse amplitude of the Ca^{2+} increase (A^{-1}) (Fig. 5*Bi*) showed that *Prnp*$^{0/0}$ neurons had a greater Ca^{2+} buffering capacity (*Prnp*$^{+/+}$: 38 ± 10; *Prnp*$^{0/0}$: 89 ± 11, $p < 0.005$). Estimates of the Ca^{2+} signaling profile in the absence of exogenous buffering showed that the peak increase was significantly smaller in *Prnp*$^{0/0}$ neurons than in *Prnp*$^{+/+}$ neurons (0.51 ± 0.05 μM and 1.10 ± 0.13 μM, respectively, $p < 0.001$). The decay rate at $\kappa'_B = 0$ was significantly slower in *Prnp*$^{0/0}$ neurons than wild type (0.37 ± 0.03 s and 0.22 ± 0.03 s, respectively, $p < 0.005$).

The Fura-2 loading experiments also allow estimation of κ_S by analyzing the depolarization evoked fluorescence decrements (ΔF_{380}). κ_S can be obtained by expressing the fluorescence decrements ΔF_{380} as a function of κ'_B (Helmchen et al., 1996). Estimates of κ_S suggested that *Prnp*$^{0/0}$ neurons (78 ± 13) have greater buffering capacity than wild-type neurons (38 ± 6, $p < 0.05$) (data not shown), consistent with the results from the inverse amplitude method.

The above Ca^{2+} buffering experiments are based on a one-compartment model and rely on the assumption that the decay of the Ca^{2+} signal is described by a single extrusion rate (Eq. 4). This assumption is supported by the observation that the decay of the Ca^{2+} transient was described by a single exponential (Fig. 5). Furthermore, the decay rate depended linearly on κ_B as predicted by Equation 4 (Fig. 5*Bii*). The extrusion of Ca^{2+} (γ) is a function of multiple mechanisms including active Ca^{2+} transport across the plasma membrane and uptake into intracellular organelles including the endoplasmic reticulum (ER) and mitochondria. Estimating γ from Equation 4 gave an extrusion rate for *Prnp*$^{+/+}$ neurons of 123 ± 16 s^{-1} ($n = 8$). In contrast, the extrusion rate for *Prnp*$^{0/0}$ neurons was significantly faster (240 ± 23 s^{-1}; $n = 8$; $p < 0.001$) (Fig. 5*D*), suggesting that *Prnp*$^{0/0}$ neurons have an enhanced extrusion mechanism.

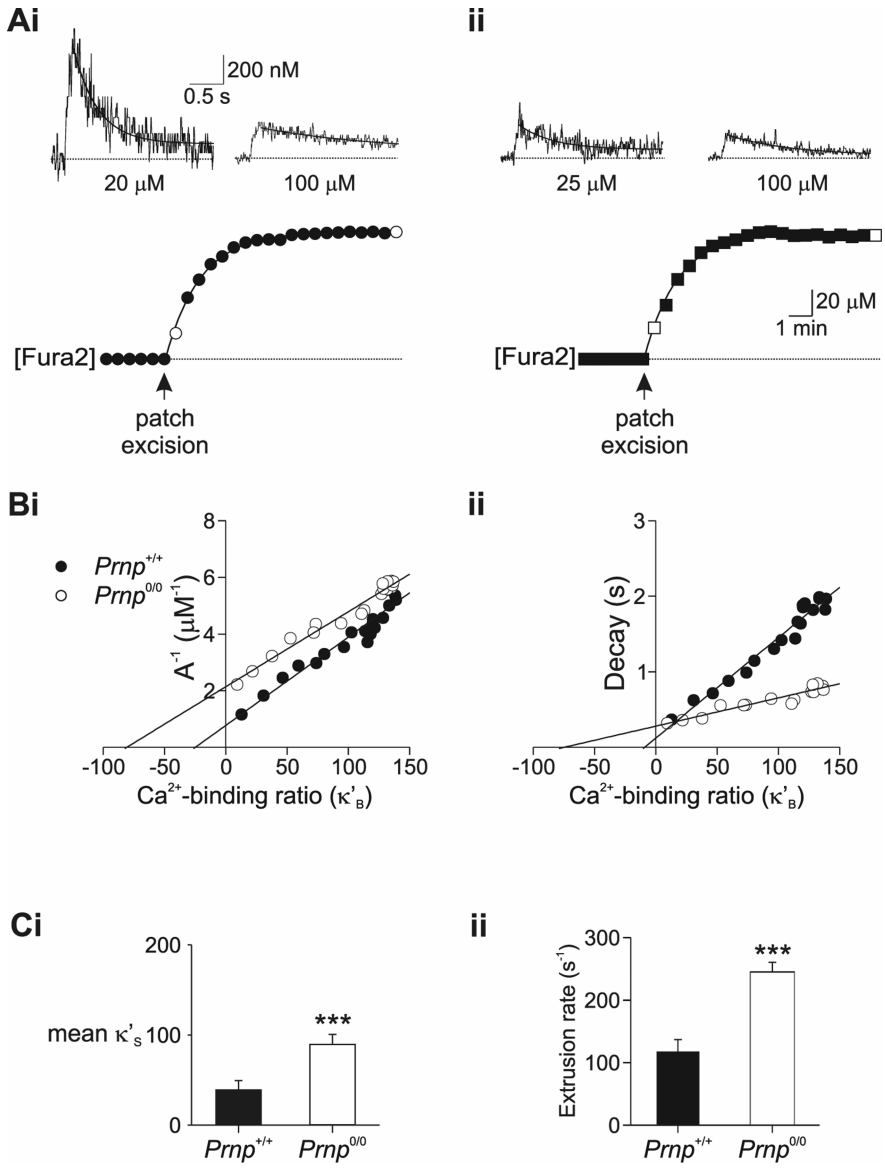

Figure 5. Endogenous Ca^{2+} buffering is enhanced in *Prnp*$^{0/0}$ neurons. Calcium buffering of CA1 neurons was assessed by monitoring calcium changes during Fura-2 loading. ***Ai***, The soma of a *Prnp*$^{+/+}$ CA1 pyramidal neuron was loaded with 100 μM Fura-2 (bottom). Measurements of depolarization-evoked somatic $[Ca^{2+}]_i$ transients were made every 30 s during loading (filled circles). $[Ca^{2+}]_i$ transients measured directly after patch excision and after full loading (open circles) are shown in the top. The Ca^{2+} transients decayed with time courses of 0.37 and 1.82 s, respectively. ***Aii***, Ca^{2+} buffering analysis for a *Prnp*$^{0/0}$ neuron during loading with 100 μM Fura2 (bottom). The Ca^{2+} transients measured immediately after patch excision and after full loading (top, open square), decayed with time courses of 0.316 and 0.828 s, respectively. ***Bi***, Inverse amplitude of Ca^{2+} changes plotted as a function of Fura-2 Ca^{2+} binding ratio (κ'_B) for individual cells. Negative *x*-axis intercepts were 25 (*Prnp*$^{+/+}$; ●) and 81 (*Prnp*$^{0/0}$; ○). ***Bii***, Decay time constant (τ) plotted as a function of Fura-2 Ca^{2+} binding ratio (κ'_B). Negative *x*-axis intercepts were 10 (*Prnp*$^{+/+}$) and 75 (*Prnp*$^{0/0}$), which is a measure of the ability of the neuron to buffer free Ca^{2+}. ***Ci***, Plot of mean endogenous binding Ca^{2+} binding ratio (κ_S) derived from inverse amplitude illustrating improved Ca^{2+} buffering in *Prnp*$^{0/0}$ neurons (means of 8 *Prnp*$^{+/+}$ and 8 *Prnp*$^{0/0}$ cells). ***Cii***, Plot of mean Ca^{2+} extrusion rate (γ) obtained from Equation 4 showing increased Ca^{2+} extrusion in *Prnp*$^{0/0}$ neurons. ***$p < 0.01$.

We explored the mechanisms responsible for the increased Ca^{2+} buffering capacity and the consequent reduction in slow AHP in *Prnp*$^{0/0}$ mice. Ca^{2+} buffering mechanisms in neurons include: extrusion across plasma membrane, binding to mobile and immobile cytoplasmic buffers and uptake into intracellular stores such as mitochondria and endoplasmic reticulum (Neher, 1998). The ER functions as a major Ca^{2+} uptake mechanism in neurons (Neering and McBurney, 1984; Sabatini et al., 2002; Usachev et al., 2006). This functional role for the ER coupled with the observations that PrP is widely expressed in the ER (Holscher et al., 2001), and that the ER has been implicated in the aberrant response of Prnp$^{0/0}$ neurons to oxidative stress (Krebs et al., 2007), led us to hypothesize that changes in the function of the ER may underlie the observed alterations in Ca^{2+} homeostasis. We

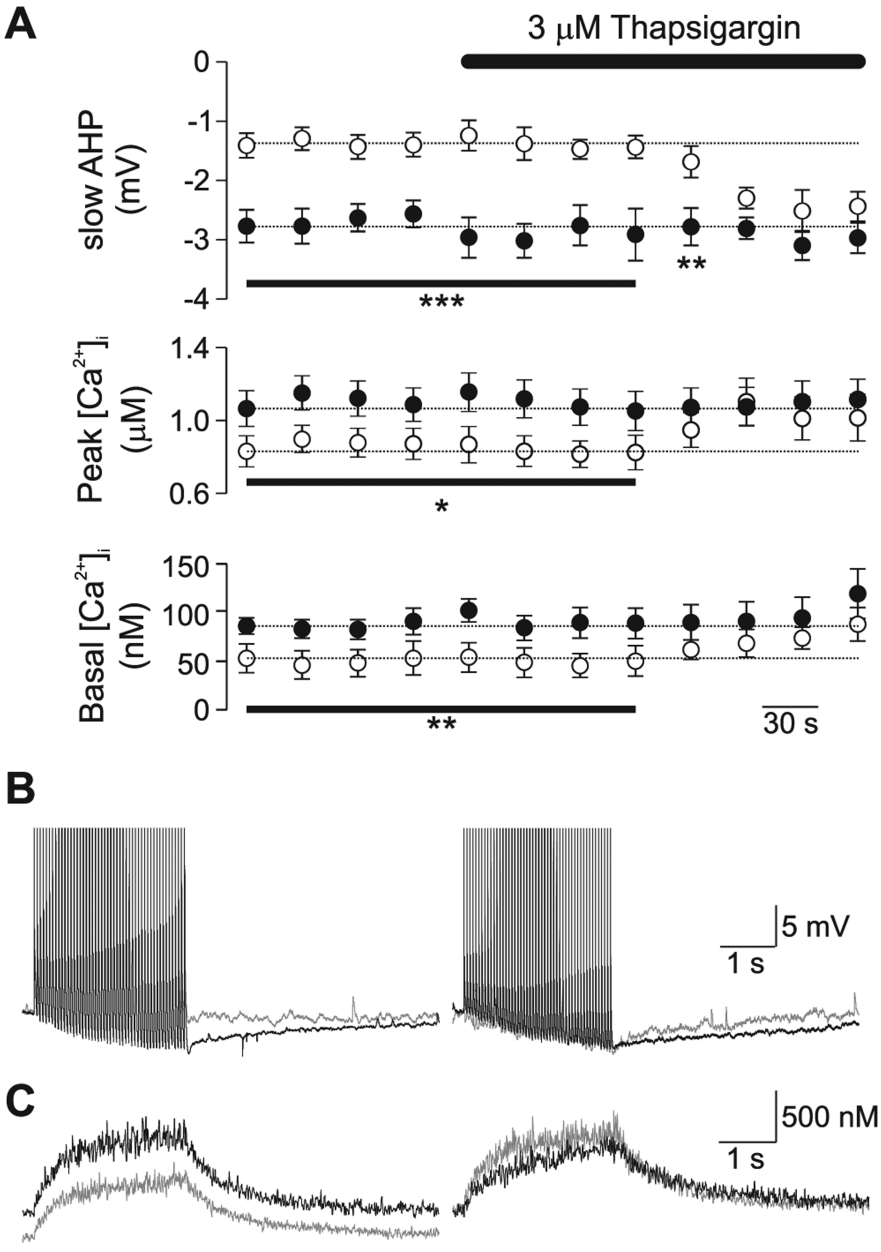

Figure 6. Block of SERCA by thapsigargin abolishes the observed changes in slow AHP and Ca^{2+} signaling $Prnp^{0/0}$ neurons. ***A***, Bath application of thapsigargin (3 μM) increased slow AHP amplitude (top), peak Ca^{2+} levels (middle), and basal Ca^{2+} levels in $Prnp^{0/0}$ neurons (open circles), but not $Prnp^{+/+}$ neurons (filled circles). ***B***, ***C***, Representative traces of voltage response (***B***) and Ca^{2+} changes (***C***) evoked by 50 action potentials at 20 Hz; control responses are shown in the left panel, thapsigargin treated responses are illustrated in the right panel ($Prnp^{0/0}$ in gray; $Prnp^{+/+}$ in black). *$p < 0.05$; **$p < 0.01$; ***$p < 0.005$.

examined the contribution of Ca^{2+} uptake into the ER by inhibiting the major ER Ca^{2+} uptake mechanism, the sarcoplasmic/endoplasmic reticulum pump Ca^{2+}-ATPase (SERCA), with either thapsigargin or cyclopiazonic acid (CPA).

Neurons were loaded with 100 μM Fura-2 for 10 min to allow the dye to equilibrate between the patch pipette and cell (Fig. 5*A*). Then, using the standard stimulation protocol of 50 action potentials delivered at 20 Hz, changes in slow AHP, basal and peak Ca^{2+} levels were monitored while the slice was perfused with 3 μM thapsigargin. Before application of thapsigargin the slow AHP, basal Ca^{2+} levels and peak Ca^{2+} change were significantly smaller in $Prnp^{0/0}$ neurons (Fig. 6*A*). Application of thapsigargin, increased the amplitude of the slow AHP, and both basal and peak Ca^{2+} changes within 4 min (Fig. 6*A*), and abolished the difference between the responses from $Prnp^{0/0}$ and control neurons (Fig. 6*B*,*C*). To confirm that the reversal of the slow AHP and Ca^{2+} signaling was the result of inhibition of SERCA, we examined the effect of a second inhibitor of SERCA, CPA, on the amplitude of the slow AHP. Similar to thapsigargin (Fig. 6*A*), CPA did not affect the amplitude of the slow AHP in $Prnp^{+/+}$ neurons (control, 2.5 ± 0.3 mV; 10 μM CPA, 2.3 ± 0.3, $n = 5$; $p = 0.42$) (supplemental Fig. 2, available at www.jneurosci.org as supplemental material). In contrast, the amplitude of the slow AHP in $Prnp^{0/0}$ neurons, was initially significantly smaller than in $Prnp^{+/+}$ neurons (control, 1.5 ± 0.3 mV; $p < 0.05$). Application of 10 μM CPA increased the amplitude of the slow AHP to 2.4 ± 0.5 mV ($n = 5$), which did not significantly differ from $Prnp^{+/+}$ neurons in the presence of CPA ($p = 0.9$). Similarly, CPA (10 μM) increased the amplitude of I_{sAHP} in $Prnp^{0/0}$ neurons (control 43.5 ± 5.9 pA, CPA 105.8 ± 24.8 pA, $n = 4$, $p < 0.05$), but not in $Prnp^{+/+}$ neurons (control 127.4 ± 17.8 pA, CPA 108.1 ± 9.1 pA).

These data suggest that the observed differences from $Prnp^{0/0}$ neurons are the result of an alteration in SERCA activity. To examine the role of SERCA in Ca^{2+} buffering further, we used the added buffer method described above. Neurons were pretreated with thapsigargin (3 μM) for 10 min before establishing a whole-cell recording and performing an added-buffer experiment. In thapsigargin naive neurons, the I_{sAHP}, basal Ca^{2+} and peak Ca^{2+} levels were significantly smaller in $Prnp^{0/0}$ neurons than control (Fig. 7*A*, Table 1). In contrast, these responses in thapsigargin pretreated $Prnp^{0/0}$ neurons were not significantly different from $Prnp^{+/+}$ responses (Fig. 7*A*, Table 1). Thapsigargin-naive $Prnp^{0/0}$ neurons showed a significantly greater κ_S (estimated from the inverse amplitude) than control neurons (80 ± 9 and 37 ± 7, respectively; $n = 11$) (Fig. 5). Inhibition of SERCA by thapsigargin did not affect κ_S in control neurons (28 ± 5; $n = 8$; $p = 0.37$). In contrast, inhibition of SERCA by thapsigargin significantly shifted the κ_S in $Prnp^{0/0}$ neurons (19 ± 4; $n = 7$; $p < 0.001$) (Fig. 7*B*,*C*), toward that observed in control neurons. Calculation of the extrusion rate revealed that pretreatment with thapsigargin reversed the increase in extrusion rate observed in $Prnp^{0/0}$ neurons (thapsigargin naïve, 240 ± 23 s^{-1}; thapsigargin, 51 ± 11 s^{-1}; $p < 0.001$). In contrast, thapsigargin did not alter the extrusion rate in $Prnp^{+/+}$ neurons significantly (thapsigargin naïve, 123 ± 16 s^{-1}; thapsigargin, 84 ± 10 s^{-1}; $p = 0.08$).

The endoplasmic reticulum provides a substantial mechanism for sequestration of action potential induced Ca^{2+} entry as blocking SERCA slows the decay of the Ca^{2+} signal (Sabatini et al., 2002). In the present study, inhibition of SERCA by thapsi-

gargin resulted in an approximate twofold (1.92 ± 0.14; $n = 10$) slowing of the decay of the Ca^{2+} signal in $Prnp^{+/+}$ neurons. In contrast, inhibition of SERCA in $Prnp^{0/0}$ neurons resulted in a significantly greater slowing of the Ca^{2+} decay time constant (2.84 ± 0.34; $n = 13$; $p = 0.04$), supporting the hypothesis that Ca^{2+} buffering is enhanced in $Prnp^{0/0}$ neurons as a result of enhanced SERCA activity. Similar results were observed when 300 nM thapsigargin was applied to neurons (data not shown).

The observation that the reduction in the slow AHP in $Prnp^{0/0}$ neurons could be rapidly reversed by inhibition of SERCA by either thapsigargin or CPA, in parallel with changes in the endogenous buffering, suggested that the κ_s could be used to predict the amplitude of the afterhyperpolarization. A plot of κ_s versus I_{sAHP} amplitude confirmed a linear relationship (Fig. 8*A*) (regression significant at $p < 0.001$). This relationship was maintained between genotypes and also for neurons that were pretreated with thapsigargin. A plot of I_{mAHP} amplitude versus κ_s revealed no correlation (Fig. 8*B*) (regression, $p = 0.21$).

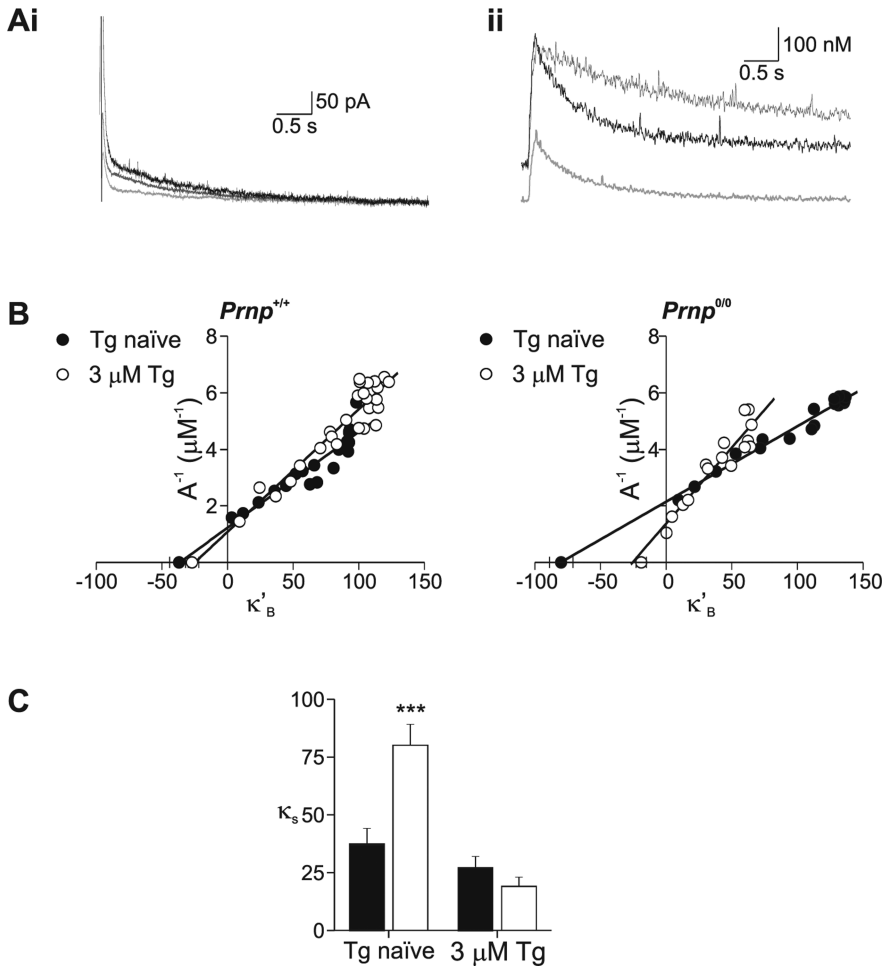

Figure 7. Block of SERCA by thapsigargin abolishes the observed changes in slow AHP, Ca^{2+} signaling, and Ca^{2+} buffering in $Prnp^{0/0}$ neurons. To examine the role of the ER in buffering, the added buffer experiments were repeated in neurons that were either under control conditions (Tg naive) or pretreated with thapsigargin (3 μM). ***A***, In $Prnp^{0/0}$ neurons, the reduction in both slow AHP (***Ai***, light gray traces) and Ca^{2+} signaling (***Aii***, light gray traces) was abolished by pretreatment with thapsigargin (3 μM; ***Ai***, ***Aii***, dark gray traces). ***B***, ***C***, Concomitant with these changes, the increase in the buffering capacity was also abolished. Buffering capacity was estimated from the inverse amplitude because blockade of SERCA alters Ca^{2+} decay kinetics. $p < 0.005$.

Discussion

Previous studies of the functional role of PrP have reported that PrP-deficient ($Prnp^{0/0}$) mice have smaller slow afterhyperpolarizations (Colling et al., 1996; Herms et al., 2001). This reduction in Ca^{2+}-activated K^+ current could arise from impairments of: Ca^{2+} channels, K^+ channels, or Ca^{2+} signaling. We identified the mechanisms responsible for the reduced AHP using a combined microfluorimetric and electrophysiological approach in CA1 pyramidal neurons.

We found no differences in Ca^{2+} currents (Herms et al., 2000; cf. Fuhrmann et al., 2006) and conclude that the weaker slow AHP must have another cause. To date, deficits in K^+ channel function have not been directly examined. If the slow AHP deficit is caused by alteration in K^+ channel function, this may arise because of alterations in the K^+ channel itself or to alterations in the putative Ca^{2+} sensor for the slow AHP, hippocalcin (Tzingounis et al., 2007). Direct activation of the Ca^{2+}-dependent K^+ channels by photorelease of caged Ca^{2+} evoked comparable AHPs in both $Prnp^{+/+}$ and $Prnp^{0/0}$ pyramidal neurons, despite the latter having significantly smaller action potential evoked slow AHPs. We therefore conclude that neither disruption of K^+ channels nor alteration in the expression of the Ca^{2+} sensor is responsible for the reduction in AHP amplitude.

The most likely explanation remaining is that $Prnp^{0/0}$ neurons have altered Ca^{2+} homeostasis, as suggested previously (Herms et al., 2000). In the present study, we found a decrease in Ca transients evoked by depolarization. We used the added buffer method to investigate this in detail (Neher, 1995; Fierro and Llano, 1996; Helmchen et al., 1996) and found that the observed alterations in Ca^{2+} signaling can be explained by increases in intracellular buffering and clearance of Ca^{2+}. The observation that the SERCA inhibitor, thapsigargin, abolished the increases in both buffering (κ_S) and clearance (γ) in $Prnp^{0/0}$ neurons suggested that the differences were caused by changes in the ER. The role of SERCA is to pump Ca^{2+} into the ER, resulting in Ca^{2+} clearance, but it also acts as a Ca^{2+} buffer (Higgins et al., 2006); both of these functions are inhibited by thapsigargin or CPA (Tadini-Buoninsegni et al., 2008). We conclude that changes in SERCA can explain increases in both buffering and clearance in the $Prnp^{0/0}$ neurons.

Aberrant ER function has been suggested previously to underlie alterations in the response of $Prnp^{0/0}$ neurons to oxidative stress (Krebs et al., 2007). Altered SERCA function may explain other phenotypes in $Prnp^{0/0}$ mice, for instance impaired LTP (Collinge et al., 1994): SERCA activity has been implicated in the induction of LTP (Harvey and Collingridge, 1992; Bardo et al., 2006), perhaps related to its effects on dendritic spine function (Scheuss et al., 2006).

In summary, we have shown that $Prnp^{0/0}$ neurons possess a reduced slow afterhyperpolarization that is a consequence of increased Ca^{2+} buffering in the endoplasmic reticulum resulting from increased SERCA activity. We propose that the increased Ca^{2+} buffering provides a mechanism for several previously reported phenotypes in prion null neurons.

Table 1. Comparison of slow AHP and Ca^{2+} signalling changes in thapsigargin naive and thapsigargin pretreated *Prnp*$^{+/+}$ and *Prnp*$^{0/0}$ neurons

	Tg naive		Tg pretreated (3 μM)	
	Prnp$^{+/+}$	*Prnp*$^{0/0}$	*Prnp*$^{+/+}$	*Prnp*$^{0/0}$
I_{sAHP} (pA)	38.9 ± 4.8	10.6 ± 3.2**	37.6 ± 5.9	39.5 ± 8.3
Basal Ca^{2+} (nM)	166.8 ± 13.0	121.7 ± 8.3*	152.2 ± 9.7	161.7 ± 15.2
Peak Ca^{2+} (μM)	0.71 ± 0.09	0.37 ± 0.05*	0.70 ± 0.11	0.81 ± 0.15

I_{sAHP} was evoked by a 50 ms somatic depolarization. Values are mean ± SEM. *$p < 0.05$; **$p < 0.01$.

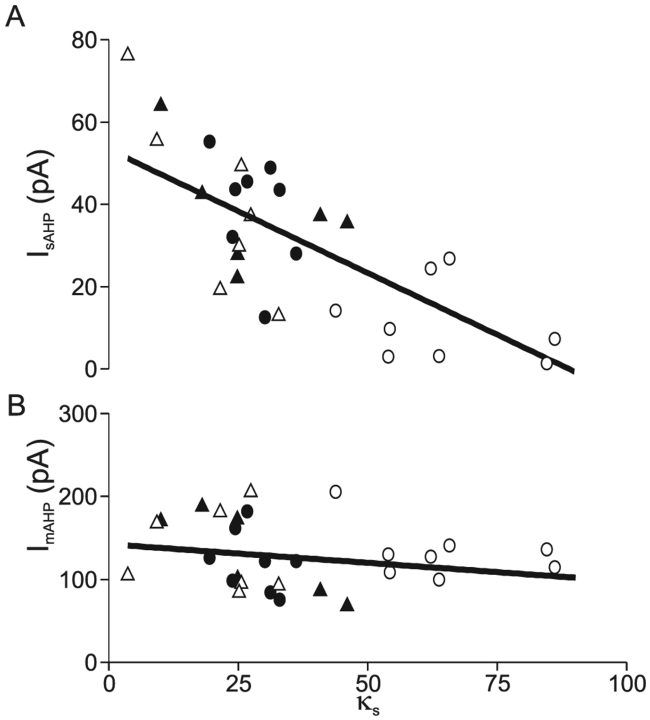

Figure 8. Slow afterhyperpolarization amplitude is correlated with endogenous buffering capacity. ***A***, Plot of slow AHP amplitude versus endogenous buffering capacity (κ_s) reveals a linear relationship (coefficient of determination 0.54; $p < 0.001$). ***B***, The medium AHP was not correlated to endogenous buffering capacity (coefficient of determination 0.022; $p = 0.21$). Filled symbols, *Prnp* $^{+/+}$; open symbols, *Prnp*$^{0/0}$; circles, thapsigargin naive; triangles, pretreated with 3 μM thapsigargin.

References

Bardo S, Cavazzini MG, Emptage N (2006) The role of the endoplasmic reticulum Ca^{2+} store in the plasticity of central neurons. Trends Pharmacol Sci 27:78–84.

Bond CT, Herson PS, Strassmaier T, Hammond R, Stackman R, Maylie J, Adelman JP (2004) Small conductance Ca^{2+}-activated K^+ channel knock-out mice reveal the identity of calcium-dependent afterhyperpolarization currents. J Neurosci 24:5301–5306.

Brini M, Miuzzo M, Pierobon N, Negro A, Sorgato MC (2005) The prion protein and its paralogue Doppel affect calcium signaling in Chinese hamster ovary cells. Mol Biol Cell 16:2799–2808.

Brown DR (2002) Copper and prion diseases. Biochem Soc Trans 30:742–745.

Bueler H, Fischer M, Lang Y, Bluethmann H, Lipp HP, DeArmond SJ, Prusiner SB, Aguet M, Weissmann C (1992) Normal development and behaviour of mice lacking the neuronal cell-surface PrP protein. Nature 356:577–582.

Carleton A, Tremblay P, Vincent JD, Lledo PM (2001) Dose-dependent, prion protein (PrP)-mediated facilitation of excitatory synaptic transmission in the mouse hippocampus. Pflügers Arch 442:223–229.

Chiarini LB, Freitas AR, Zanata SM, Brentani RR, Martins VR, Linden R (2002) Cellular prion protein transduces neuroprotective signals. EMBO J 21:3317–3326.

Colling SB, Collinge J, Jefferys JGR (1996) Hippocampal slices from prion protein null mice: disrupted Ca^{2+}-activated K^+ currents. Neurosci Lett 209:49–52.

Colling SB, Khana M, Collinge J, Jefferys JGR (1997) Mossy fibre reorganization in the hippocampus of prion protein null mice. Brain Res 755:28–35.

Collinge J (2001) Prion diseases of humans and animals: their causes and molecular basis. Annu Rev Neurosci 24:519–550.

Collinge J, Whittington MA, Sidle KCL, Smith CJ, Palmer MS, Clarke AR, Jefferys JGR (1994) Prion protein is necessary for normal synaptic function. Nature 370:295–297.

Davies P, Brown DR (2008) The chemistry of copper binding to PrP: is there sufficient evidence to elucidate a role for copper in protein function? Biochem J 410:237–244.

Faas GC, Karacs K, Vergara JL, Mody I (2005) Kinetic properties of DM-nitrophen binding to calcium and magnesium. Biophys J 88:4421–4433.

Fierro L, Llano I (1996) High endogenous calcium buffering in Purkinje cells from rat cerebellar slices. J Physiol (Lond) 496:617–625.

Fournier JG, Escaig-Haye F, Grigoriev V (2000) Ultrastructural localization of prion proteins: physiological and pathological implications. Microsc Res Tech 50:76–88.

Fuhrmann M, Bittner T, Mitteregger G, Haider N, Moosmang S, Kretzschmar H, Herms J (2006) Loss of the cellular prion protein affects the Ca^{2+} homeostasis in hippocampal CA1 neurons. J Neurochem 98:1876–1885.

Grynkiewicz G, Poenie M, Tsien RY (1985) A new generation of Ca^{2+} indicators with greatly improved fluorescence properties. J Biol Chem 260:3440–3450.

Harvey J, Collingridge GL (1992) Thapsigargin blocks the induction of long-term potentiation in rat hippocampal slices. Neurosci Lett 139:197–200.

Helmchen F, Imoto K, Sakmann B (1996) Ca^{2+} buffering and action potential-evoked Ca^{2+} signaling in dendrites of pyramidal neurons. Biophys J 70:1069–1081.

Herms J, Tings T, Gall S, Madlung A, Giese A, Siebert H, Schurmann P, Windl O, Brose N, Kretzschmar H (1999) Evidence of presynaptic location and function of the prion protein. J Neurosci 19:8866–8875.

Herms JW, Korte S, Gall S, Schneider I, Dunker S, Kretzschmar HA (2000) Altered intracellular calcium homeostasis in cerebellar granule cells of prion protein-deficient mice. J Neurochem 75:1487–1492.

Herms JW, Tings T, Dunker S, Kretzschmar HA (2001) Prion protein affects Ca^{2+}-activated K^+ currents in cerebellar Purkinje cells. Neurobiol Dis 8:324–330.

Holscher C, Bach UC, Dobberstein B (2001) Prion protein contains a second endoplasmic reticulum targeting signal sequence located at its C terminus. J Biol Chem 276:13388–13394.

Higgins ER, Cannell MB, Sneyd J (2006) A buffering SERCA pump in models of calcium dynamics. Biophys J 91:151–163.

Hutter G, Heppner FL, Aguzzi A (2003) No superoxide dismutase activity of cellular prion protein in vivo. Biol Chem 384:1279–1285.

Jones S, Batchelor M, Bhelt D, Clarke AR, Collinge J, Jackson GS (2005) Recombinant prion protein does not possess SOD-1 activity. Biochem J 392:309–312.

Krebs B, Wiebelitz A, Balitzki-Korte B, Vassallo N, Paluch S, Mitteregger G, Onodera T, Kretzschmar HA, Herms J (2007) Cellular prion protein modulates the intracellular calcium response to hydrogen peroxide. J Neurochem 100:358–367.

Lancaster B, Adams PR (1986) Calcium-dependent current generating the afterhyperpolarization of hippocampal neurons. J Neurophysiol 55:1268–1282.

Lancaster B, Zucker RS (1994) Photolytic manipulation of Ca^{2+} and the time course of slow, Ca^{2+}-activated K^+ current in rat hippocampal neurones. J Physiol (Lond) 475:229–239.

Mallucci GR, Ratte S, Asante EA, Linehan J, Gowland I, Jefferys JG, Collinge J (2002) Post-natal knockout of prion protein alters hippocampal CA1 properties, but does not result in neurodegeneration. EMBO J 21:202–210.

Manson JC, Hope J, Clarke AR, Johnston A, Black C, MacLeod N (1995) PrP gene dosage and long term potentiation. Neurodegeneration 4:113–114.

Maravall M, Mainen ZF, Sabatini BL, Svoboda K (2000) Estimating intra-

cellular calcium concentrations and buffering without wavelength rationing. Biophys J 78:2655–2667.
Neering IR, McBurney RN (1984) Role for microsomal Ca storage in mammalian neurones? Nature 309:158–160.
Neher E (1995) The use of fura-2 for estimating Ca buffers and Ca fluxes. Neuropharmacology 34:1423–1442.
Neher E (1998) Usefulness and limitations of linear approximations to the understanding of Ca^{2+} signals. Cell Calcium 24:345–357.
Palecek J, Lips MB, Keller BU (1999) Calcium dynamics and buffering in motoneurones of the mouse spinal cord. J Physiol (Lond) 520:485–502.
Pedarzani P, McCutcheon JE, Rogge G, Jensen BS, Christophersen P, Hougaard C, Strobaek D, Stocker M (2005) Specific enhancement of SK channel activity selectively potentiates the afterhyperpolarizing current I_{AHP} and modulates the firing properties of hippocampal pyramidal neurons. J Biol Chem 280:41404–41411.
Prusiner SB (1998) Prions. Proc Natl Acad Sci USA 95:13363.
Rieger R, Edenhofer F, Lasmezas CI, Weiss S (1997) The human 37-kDa laminin receptor precursor interacts with the prion protein in eukaryotic cells. Nat Med 3:1383–1388.
Sabatini BL, Oertner TG, Svoboda K (2002) The life cycle of Ca^{2+} ions in dendritic spines. Neuron 33:439–452.
Sah P, Clements JD (1999) Photolytic manipulation of $[Ca^{2+}]_i$ reveals slow kinetics of potassium channels underlying the afterhyperpolarization in hippocampal pyramidal neurons. J Neurosci 19:3657–3664.
Sah P, Faber ES (2002) Channels underlying neuronal calcium-activated potassium currents. Prog Neurobiol 66:345–353.
Scheuss V, Yasuda R, Sobczyk A, Svoboda K (2006) Nonlinear $[Ca^{2+}]$ signaling in dendrites and spines caused by activity-dependent depression of Ca^{2+} extrusion. J Neurosci 26:8183–8194.
Tadini-Buoninsegni F, Bartolommei G, Moncelli MR, Tal DM, Lewis D, Inesi G (2008) Effects of high-affinity inhibitors on partial reactions, charge movements and conformational states of the Ca^{2+} transport ATPase (sarcoendoplasmic reticulum Ca^{2+} ATPase). Mol Pharm 73:1134–1140.
Tzingounis AV, Kobayashi M, Takamatsu K, Nicoll RA (2007) Hippocalcin gates the calcium activation of the slow afterhyperpolarization in hippocampal pyramidal cells. Neuron 53:487–493.
Usachev YM, Marsh AJ, Johanns TM, Lemke MM, Thayer SA (2006) Activation of protein kinase C in sensory neurons accelerates Ca^{2+} uptake into the endoplasmic reticulum. J Neurosci 26:311–318.
Watt NT, Hooper NM (2003) The prion protein and neuronal zinc homeostasis. Trends Biochem Sci 28:406–410.